

Development of a shear band cleavage as a result of strain partitioning

Katsuyoshi Michibayashi*, Masami Murakami

Institute of Geosciences, Shizuoka University, Ohya 836, Suruga-ku, Shizuoka 422-8529, Japan

Received 23 March 2006; received in revised form 18 January 2007; accepted 5 February 2007
Available online 20 February 2007

Abstract

Microstructural analyses of shear band cleavages in a centimeter-scale shear zone within a metasomatic biotite band in the Teshima granite, Ryoke metamorphic belt, southwest Japan, show that strain partitioning occurred between quartz and biotite-feldspar domains within the shear zone. Pre-tectonic hydrothermal alteration within the granite caused biotite replacement of both plagioclase and K-feldspar, resulting in the development of biotite-feldspar domains where K-feldspar mantles dominantly biotite-plagioclase aggregates. Subsequently, the altered granite was plastically deformed in simple shear, so that intra-layer shear band cleavages were passively developed within the biotite-feldspar domains, whereas intense dynamic recrystallization occurred in the quartz domains. The rotation and orientation of the intra-layer shear band cleavages can be explained by a finite strain ellipse model, which shows that strain in the biotite-feldspar domain requires only 10–20% of the bulk simple shear strain for the development of such cleavages, so that most of strain could be accommodated by deformation in the quartz domain. Consequently, the model suggests that the development of the shear zone resulted in strain partitioning between the quartz and the biotite-feldspar domains due to compositional variations via hydrothermal alteration within the granite.

© 2007 Elsevier Ltd. All rights reserved.

Keywords: Shear band cleavage; shear zone; strain partitioning; alteration; granite; strain analysis; Ryoke metamorphic belt

1. Introduction

Within deformed rocks, a mica-preferred orientation or compositional layering may be transected at a small angle by sets of subparallel minor shear zones, known as shear band cleavages (Passchier and Trouw, 2005). Shear band cleavages are commonly slightly oblique to the direction of shear, and have been variously referred to as C' -surfaces (e.g., Berthé et al., 1979; Blenkinsop and Treloar, 1995; Pray et al., 1997), shear bands (White et al., 1980; Gapais and White, 1982), extensional crenulation cleavage (Platt and Vissers, 1980) and normal slip crenulation (Dennis and Secor, 1987). Shear band cleavages are extensively used as shear sense indicators in shear zones (e.g., Berthé et al., 1979; Lister and Snoke, 1984), although their development

is not fully understood (Passchier and Trouw, 2005). This is because it is difficult to obtain reliable data from natural shear zones on factors such as deformation history, initial orientation of shear bands, bulk and local finite strain, and bulk and local volume change (Passchier, 1991).

In this paper, we conducted a simple geometric analysis of shear band cleavages along a strain gradient from the margin to the centre of a centimeter-scale shear zone. As a result, we demonstrate that a finite strain ellipse model proposed by Platt (1984) could explain the development of shear band cleavages in this small shear zone.

2. Regional geology and sample description

The sample analysed in this study was collected from Teshima island in the Shiwaku Island Group, Japan, within the Ryoke HT/LP metamorphic belt (Fig. 1; e.g., Hara et al., 1973; Arita, 1988). Gneissic coarse-grained hornblende-biotite

* Corresponding author. Tel.: +81 54 238 4788; fax: +81 54 238 0491.
E-mail address: sekmich@ipc.shizuoka.ac.jp (K. Michibayashi).

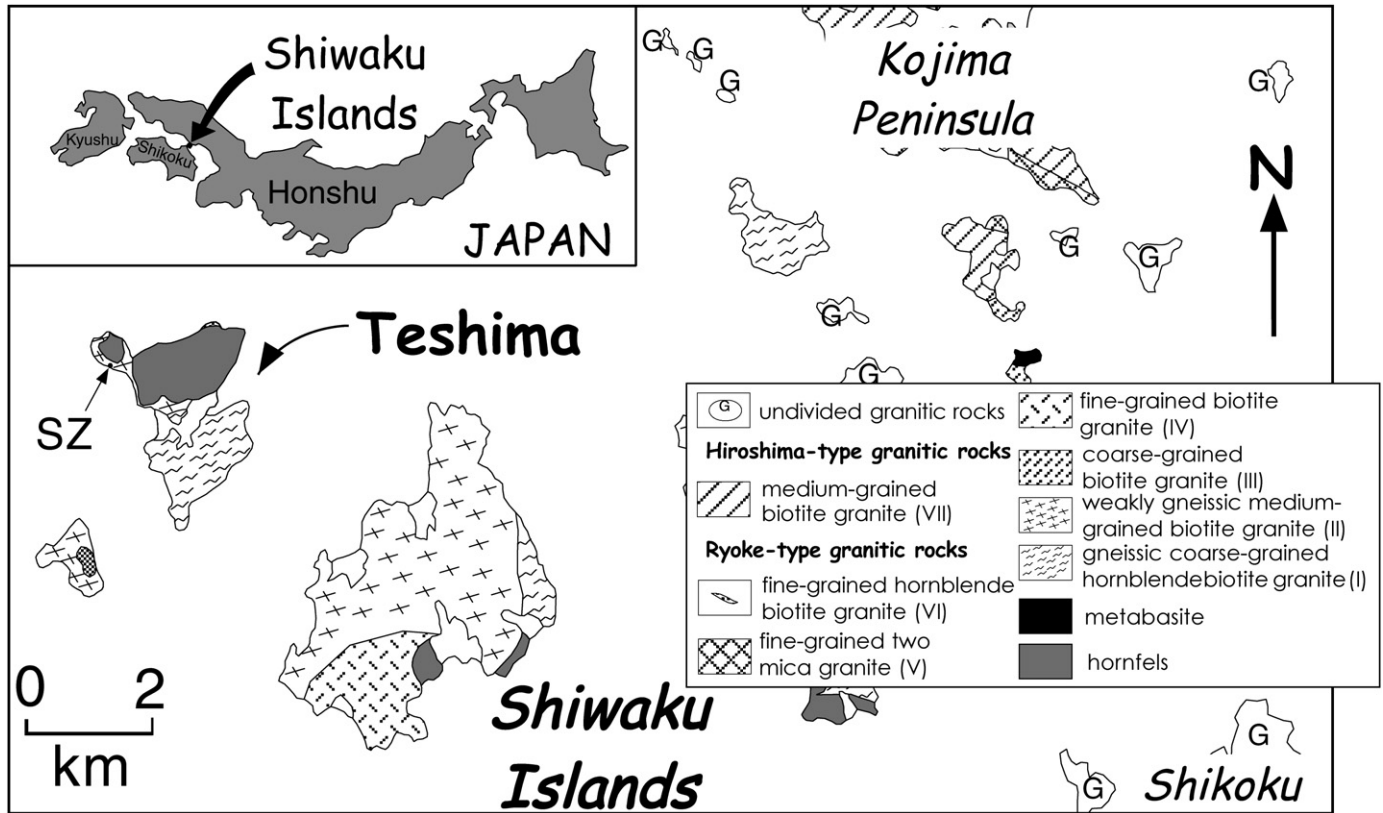


Fig. 1. Geological map of the Shiwaku Islands, SW Japan. Teshima island consists of Ryoke-type granitic rocks and hornfels (Arita, 1988). The sample studied in this paper was taken from the NW side of this island at the locality 'SZ'.

granite occurs in the south of the island, and weakly gneissic medium-grained biotite granite and hornfels occur in the north of the island (Fig. 1; Arita, 1988).

The introduction of iron-bearing fluid phases resulted in hydrofracturing in the northwestern part of the biotite granite and the formation of thin metasomatic biotite bands (thickness: 5–10 cm), some of which contain quartz veins in the middle of the bands (thickness: 1–4 cm); the biotite bands are sub-vertical and strike approximately 20° (Michibayashi et al., 1999). The bands locally occur as anastomosing networks. The bands resulted from biotite replacement of mainly plagioclase and K-feldspar grains with the addition of iron-bearing fluids (Fig. 2). The mineral replacements weakened this part of the granite, and small-scale sinistral shear zones developed within those parts of the granite that contain quartz veins and biotite bands (Michibayashi et al., 1999).

The analysed sample was taken from a metasomatic biotite band, and contains one side of a shear zone, where a shear plane of the shear zone centre is subparallel to the strike and dip of the biotite band (Fig. 2). The protolith is a medium-grained biotite granite, which consists of quartz, plagioclase, K-feldspar and biotite, with minor zircon and muscovite. EPMA chemical analysis revealed that plagioclase grains are An_{5-16} , K-feldspar grains are Or_{92-96} , and biotite grains are iron-rich, with $Mg/(Fe + Mg) = 0.05-0.07$ (Togami et al., 2000).

In the sampled rock, biotite layers define a foliation within the biotite band, which shows some degree of obliquity with

respect to the centre of the shear zone (Fig. 2). This obliquity provides a continuous gradient from high angle at relatively unstrained to low angle at highly deformed over a distance of several centimeters. Here, we define a distance (d) normal to the shear plane of the shear zone centre ($d = 0$).

3. Microstructures

Element mapping by X ray fluorescence studied by Michibayashi et al. (1999) showed that quartz modal composition increases toward the centre of the shear zone. Michibayashi et al. (1999) defined the three domains according to a zonation in the metasomatised band: the quartz domain, biotite domain and K-feldspar domain. In this paper, although we study the microstructures that occur mostly in the quartz domain and partly in the biotite domain of Michibayashi et al. (1999), it is rather convenient to re-divide microstructures within these two domains into two dominant domains: quartz domains and biotite-feldspar domains as follows.

3.1. Quartz domains

The quartz domains contain quartz grains with feldspar inclusions and become more dominant toward the centre of the shear zone. Modal composition analysis showed that modal composition of the quartz domain increases from the biotite band to the centre of the shear zone by up to 60% (Michibayashi et al., 1999).

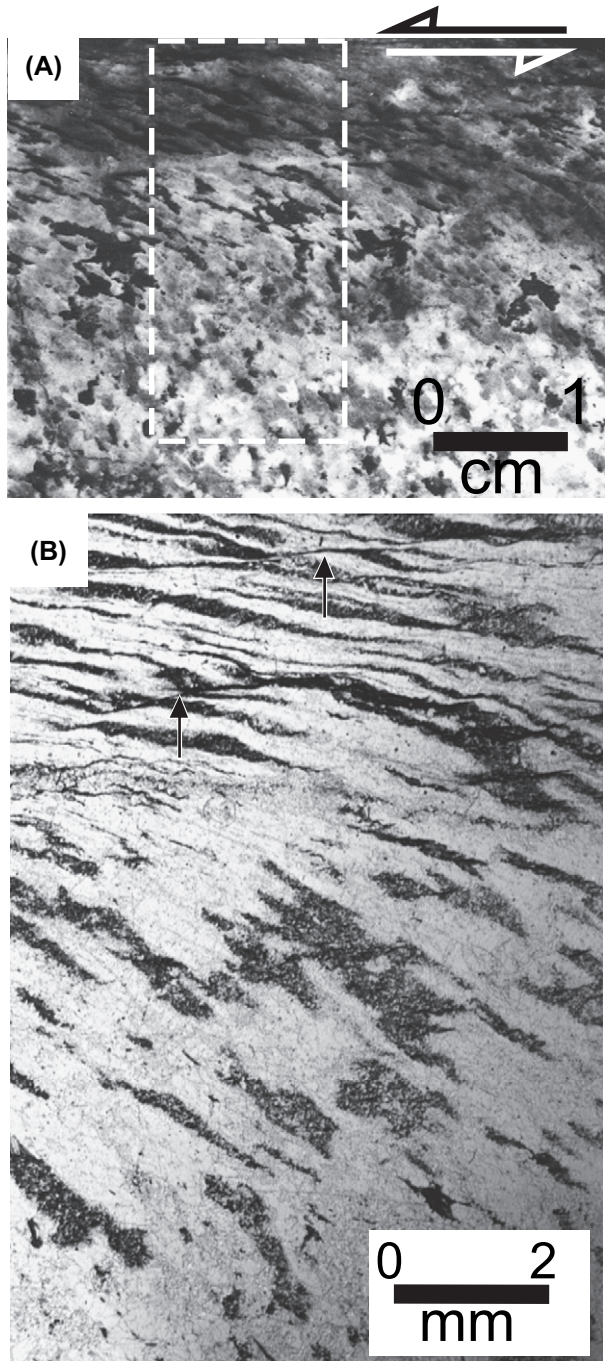


Fig. 2. (A) A rock slab of a small-scale shear zone studied in this paper. The square underlined by a broken line shows the position of the thin section in (B). (B) Photomicrograph of one side of the shear zone within the biotite band. Plane-polarized light. Dark biotite-feldspar domains are gradually elongated and rotated toward the shear plane. The intra-layer shear band cleavages occur within the dark elongated biotite-plagioclase layers, whereas the inter-layer shear band cleavages cut across both the biotite-feldspar and quartz layers (arrows for example).

Fig. 3A shows quartz grains within the relatively undeformed granite at $d = 15$ cm. Grains have weak serrated boundaries with stable triple points, indicating minimal deformation. At the margin of the shear zone ($d = 4$ cm), quartz grains have developed a slightly elongate shape without

formation of a foliation (Fig. 3B), indicating that bulk strain is low. At $d = 2.5$ cm, quartz grains are weakly elongate subparallel to S-foliation (Fig. 3C) and in part recrystallized, with intensely serrated grain boundaries and strong undulose extinction. At $d = 1.5$ cm, deformation in quartz is further intensified (Fig. 3D). Although igneous quartz grains are still visible, intracrystalline deformation has resulted in strong undulose extinctions and serrated grain boundaries. At $d = 1$ cm, quartz grains are intensely elongated parallel to S-foliation, and dynamic recrystallization has resulted in a reduction in grain size (Fig. 3E). The intensity of dynamic recrystallization increases toward the shear zone centre (Fig. 3F). The grain size of quartz is reduced from ca. 0.5 mm in the undeformed granite (Fig. 3A) to ca. 50 μm within the shear zone (Fig. 3F). Fine K-feldspar inclusions within the quartz domains are also elongated parallel to S-foliation.

Quartz crystal-preferred orientations (CPOs) were measured from highly polished thin section using a JEOL 6300 SEM equipped with electron back-scattered diffraction (EBSD) at Shizuoka University, Japan. Quartz CPOs show triclinic symmetries with the girdle of c -axes subparallel to the Y -axis toward the centre of the shear zone, although quartz CPOs at $d = 2.5$ – 3.5 cm have a triclinic symmetry slightly oblique to XZ plane (Fig. 4). These patterns show that prism $\langle a \rangle$ slip was dominant in this shear zone (e.g., Passchier and Trouw, 2005).

3.2. Biotite-feldspar domains

The biotite-feldspar domains consist mainly of secondary fine-grained biotite and plagioclase aggregates (Fig. 5). Michibayashi et al. (1999) showed that primary plagioclase grains occur as a matrix to the fine-grained biotite aggregates and that the biotite-feldspar domains are commonly mantled by K-feldspar (Fig. 6; see also Fig. 3 of Michibayashi et al., 1999). The amount of fine-grained biotite grains in plagioclase tends to increase toward the centre of the shear zone (Michibayashi et al., 1999). The shear band cleavages studied in this paper occur dominantly in the biotite-feldspar domains.

In the relatively undeformed granite at $d = 15$ cm, biotite occurs as randomly oriented euhedral primary grains (Fig. 5A). Secondary fine-grained biotite aggregates first occur within coarse plagioclase grains at $d = 4$ cm (Fig. 5B). Deformation is weak and the secondary biotite grains have no preferred orientation. The biotite-feldspar domains become elongated at $d = 2.5$ cm and define an S-foliation at the margin of the shear zone (solid line in Fig. 5C). The angle between the S-foliation and the shear plane is as high as 45° . However, the secondary biotite grains within plagioclase grains are randomly oriented (Figs. 5C and 6A).

The characters of the biotite-feldspar domains change gradually toward the shear zone centre. At $d = 2$ cm, the domains become elongate parallel to the S-foliation, and the secondary biotite grains are sheared, resulting in the initiation of intra-layer shear band cleavage subparallel to the shear plane (Fig. 5D). The biotite-feldspar at $d = 1$ cm where the secondary biotite have developed are further elongated parallel to the

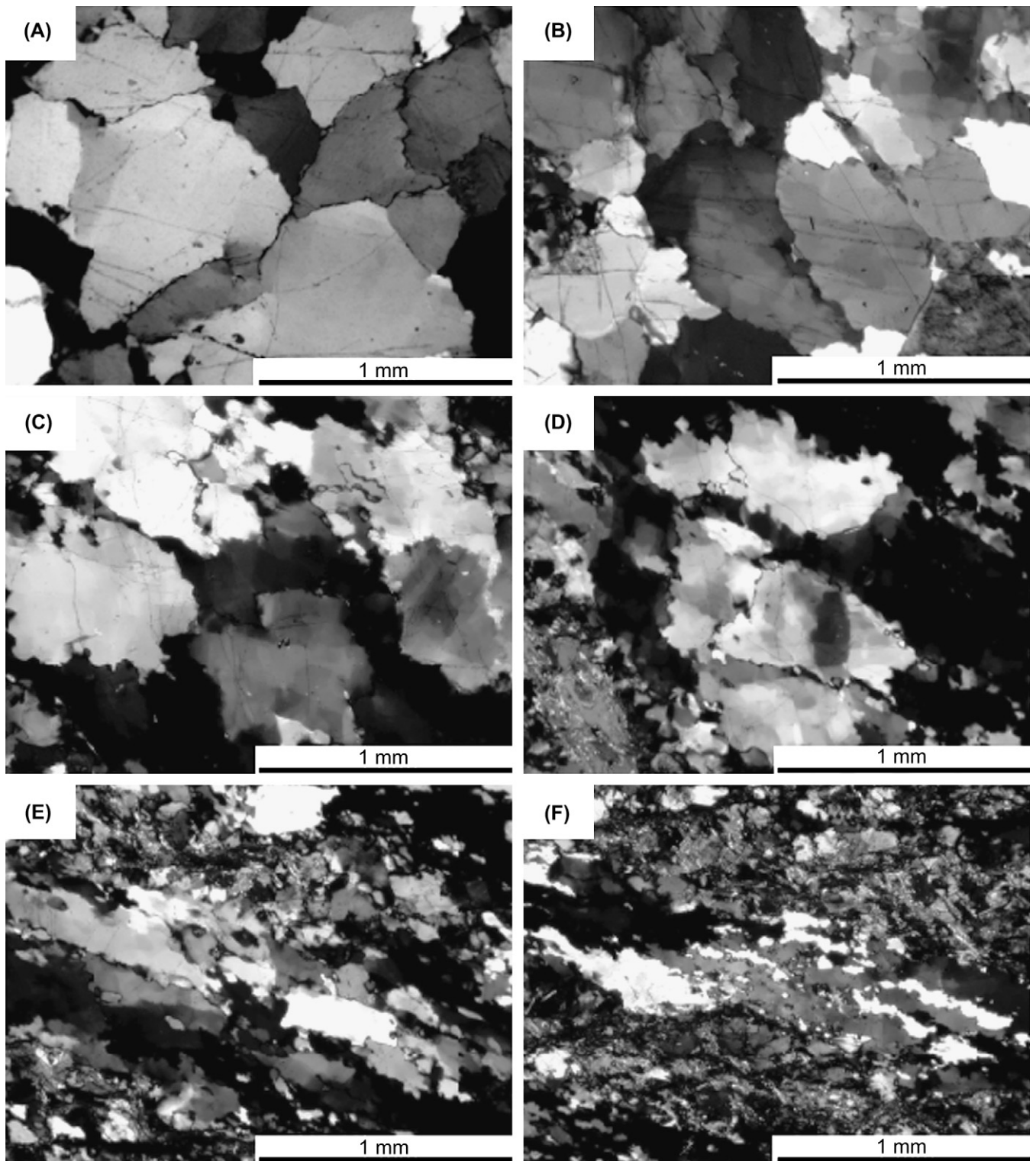


Fig. 3. Sequence of photomicrographs under crossed polars illustrating the changing shape of quartz grains from the margin to the centre of the shear zone. (A) $d = 15$ cm; (B) $d = 4$ cm; (C) $d = 2.5$ cm; (D) $d = 1.5$ cm; (E) $d = 1$ cm; (F) $d = 0.2$ cm.

S-foliation (Figs. 5E and 6B). The secondary biotite grains are intensely deformed, and many shear band cleavages have developed.

Within the centre of the shear zone, biotite-feldspar domains are strongly elongated parallel to the S-foliation (Fig. 5F) and intra-layer shear band cleavages are pervasively

developed. Although the S-foliation is oriented subparallel to the shear plane, the intra-layer shear band cleavages occur at about $10\text{--}20^\circ$ to both S-foliation and the shear plane.

The shear band cleavages described above are of the intra-layer type, as they occur only within the biotite-feldspar domains. Inter-layer type shear band cleavages also occur in

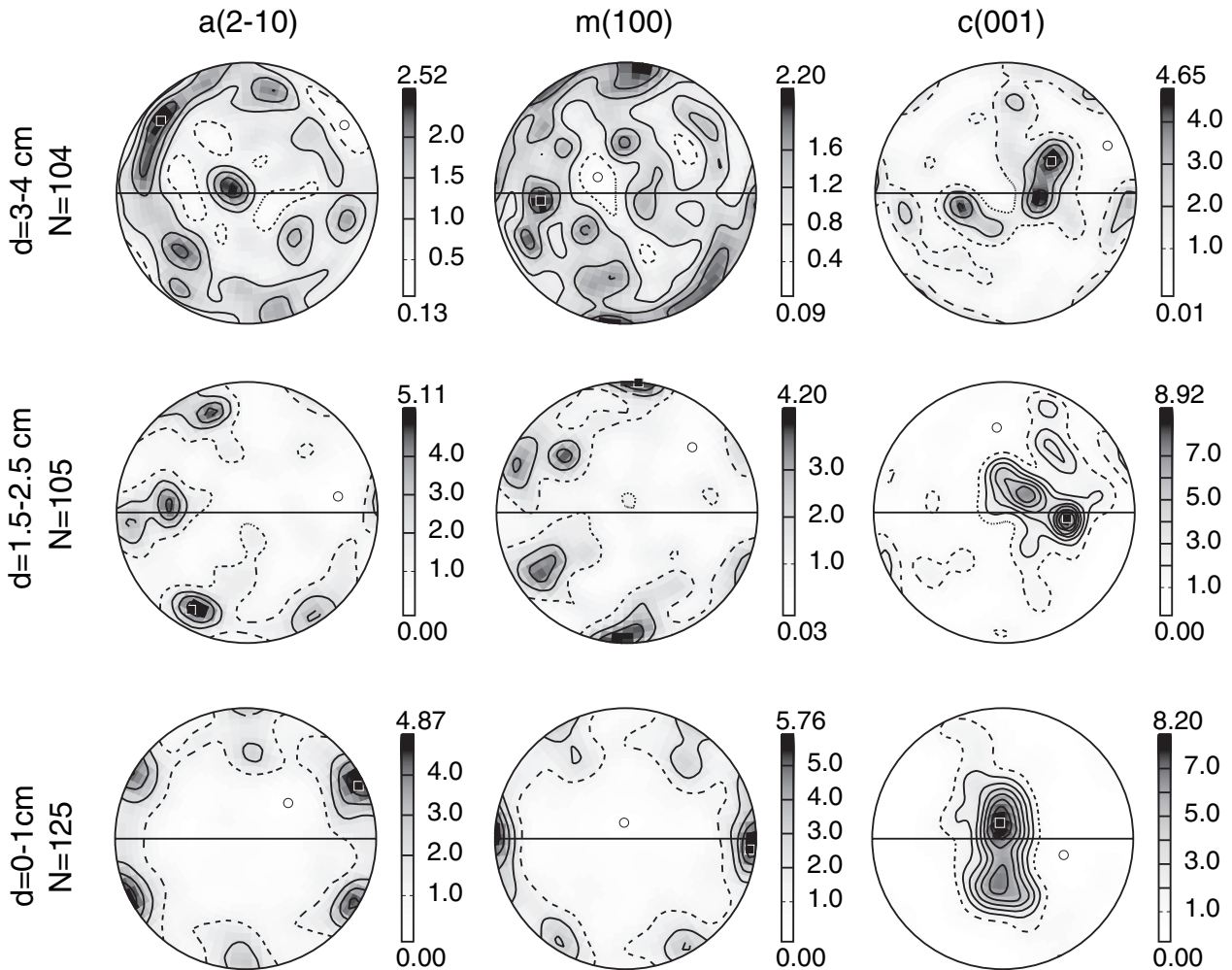


Fig. 4. Pole diagrams showing CPO patterns of quartz within the quartz domain with respect to the centre of the shear zone. Equal area projection, lower hemisphere. Contours are in multiples of uniform distribution (m.u.d.). Foliation is vertical and lineation is horizontal within the plane of the foliation.

the vicinity of the shear zone centre (Figs. 2B and 7). Displacements along the inter-layer shear band cleavages are relatively large, and cut across the biotite-feldspar domains, the quartz domains (Figs. 2B and 7) and the intra-layer shear band cleavages.

It is important to note that there is no evidence of overgrowth of any minerals on the shear band cleavages (Figs. 5 and 6). This suggests that the development of such planar fabrics occurred after the metasomatic reactions in the biotite band (e.g., Michibayashi et al., 1999).

4. Geometric analysis

4.1. Methods

We performed a microstructural analysis to investigate variations in the geometry of the shear band cleavages across the shear zone. Four parameters were measured with the aid of an optical microscope: (i) spacing of adjacent shear band cleavages, (ii) the angle between the S-foliation and the shear plane (ϕ), (iii) the angle between the shear band cleavage and the

shear plane (ψ), and (iv) the angle between the S-foliation and the shear band cleavage (η ; Fig. 8A) which equals $\phi + \psi$.

4.2. Results

Results are shown in Fig. 8B–E. Open diamonds indicate the biotite-feldspar domains where an S-foliation occurs without shear band cleavage (e.g., Fig. 5C), and in this case only one parameter (ϕ) has been measured (Fig. 8C). Solid circles represent the data for the intra-layer shear band cleavages, whereas open triangles show those for the inter-layer shear band cleavages.

Fig. 8B shows that the spacing of the intra-layer shear bands varies from 0.5 to 2 mm away from the shear zone centre, whereas it tends to be in a small range between 0.2 and 0.5 mm near the shear zone centre. Fig. 8C shows the trend of S-foliation with respect to the shear plane (ϕ) across the shear zone. Several points of biotite-feldspar domains record ϕ angles of $>45^\circ$. There is no shear band cleavage within such high-angle biotite-feldspar domains (Fig. 8C). Shear band cleavage

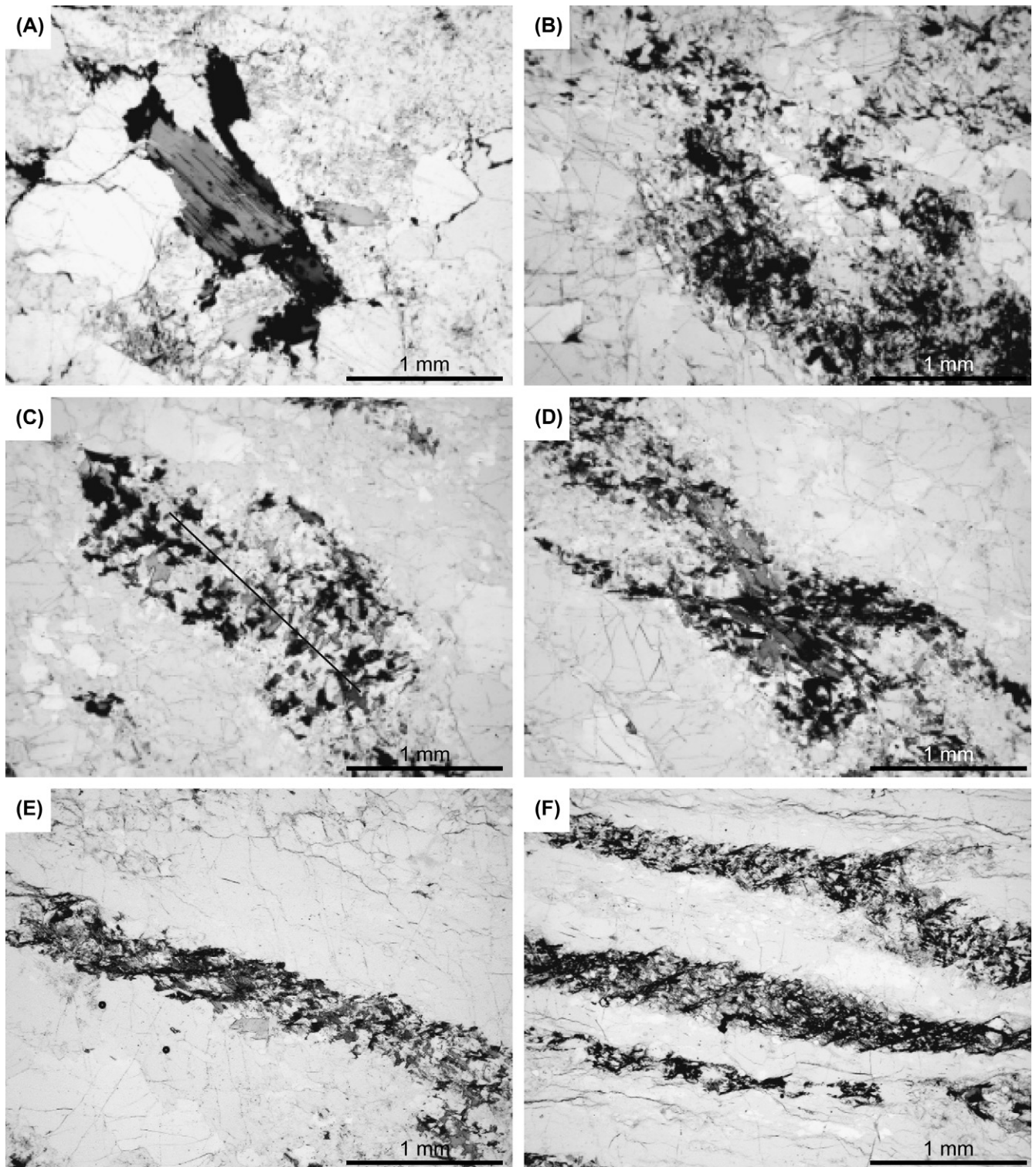


Fig. 5. Sequence of photomicrographs under plane-polarized light illustrating the changing character of biotite-feldspar domains from the margin to the centre of the shear zone. (A) Euhedral primary biotite grains within the relatively undeformed protolith granite ($d = 15$ cm). (B) Secondary fine-grained biotite aggregates within plagioclase grains ($d = 4$ cm). (C) Secondary fine-grained biotite aggregates within plagioclase grains ($d = 2.5$ cm). Weak S-foliation can be seen (solid line). (D) Secondary fine-grained biotite aggregates within plagioclase grains ($d = 1.5$ cm). Note the development of weak intra-layer shear band cleavages sub-parallel to the horizontal shear plane. (E) Secondary fine-grained biotite aggregates within plagioclase grains ($d = 1$ cm). Discrete intra-layer shear band cleavages occur. (F) Secondary fine-grained biotite aggregates within plagioclase grains ($d = 0.2$ cm). Discrete intra-layer shear band cleavages occur at high angles to the subhorizontal shear plane.

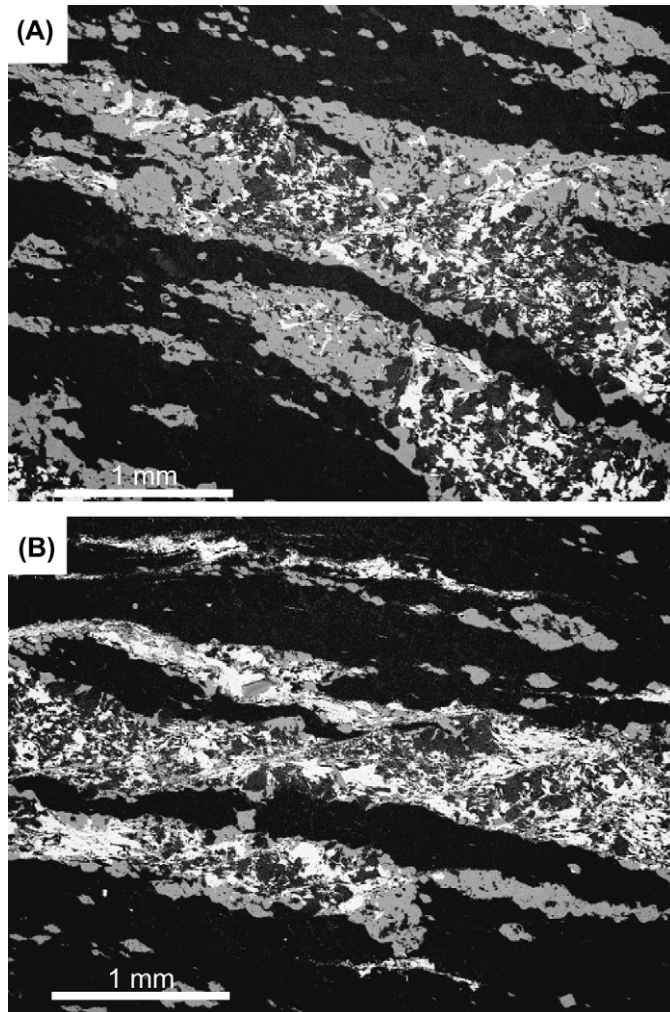


Fig. 6. Back-scattered electron images of the intra-layer shear band cleavages. The biotite-plagioclase domains (white and dark gray) are mantled by K-feldspar (light gray). (A) Approximately 2.5 cm from the shear zone centre. (B) 1 cm from the shear zone centre.

occurs where the angle of the S-foliation to the shear plane (ϕ) is less than 45° (Fig. 8C).

The angle between the intra-layer shear band cleavage and the shear plane (ψ) shows a gradual change from subparallel to

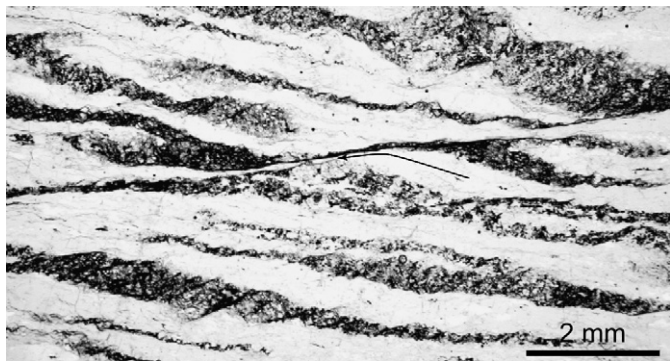


Fig. 7. Photomicrographs of the inter-layer type shear band cleavages, which cut across the biotite-feldspar domains, quartz domains and the intra-layer shear band cleavages at closer angles to the subhorizontal shear plane. The arrow indicates curvature of the quartz domain along the inter-layer cleavages.

the shear plane to negatively oblique orientation as the distance to the shear zone centre decreases (Fig. 8D). The intra-layer shear band cleavages appear for a distance $d < 10$ mm (Fig. 8D). Their angles are narrower than those of the intra-layer cleavages and show no tendency with respect to the distance from the shear zone centre. The angle between S-foliation and the shear band cleavages (η) has a scattered distribution (Fig. 8E).

In order to examine the relationship between the three parameters (ϕ, ψ, η), we made a variation diagram between ϕ and ψ (Fig. 9), where each line shows a stable value of the angle (η) as $\psi = \phi - \eta$ that is defined in Fig. 8A. It appears that the angles between the S-foliation and the shear band cleavages became somehow narrower as ϕ being smaller. Notice that the inter-layer shear band cleavages tend to occur where the intra-layer shear band cleavages are at higher angles to the shear plane.

5. Interpretation and discussion

5.1. The evolution of planar fabrics with respect to simple shear strain

From the measured spatial variations in microstructural development described above, we have sought to model temporal changes by assuming that the intra-layer shear band cleavages close to the centre of the shear zone preserve more progressively developed types than those away from the centre of the shear zone. This small-scale shear zone occurs within largely undeformed granite. Although this shear zone occurs in a metasomatic biotite band, we consider that volume change during deformation was minimal, as there is no evidence of overgrowth or dissolution of minerals on the shear band cleavages. Hara et al. (1973) examined quartz *c*-axis orientations in this area and also concluded that the shear zones formed under conditions of simple shear strain. Quartz CPOs in Fig. 4 could also result from simple shearing in quartz. Although quartz CPOs at $d = 2.5$ – 3.5 cm are slightly oblique, its triclinic symmetry is still maintained. Therefore, a simple shear strain model is a suitable first order estimation of the bulk kinematic framework. As a consequence, we interpret the development of the shear band cleavages in terms of bulk simple shear.

In general, there are two alternative interpretations of ϕ : either (i) as the direction of the instantaneous stretching axis (i.e. $\tan 2\phi = 2/\gamma$; e.g., Ramsay and Graham, 1970), or (ii) as the direction of a material line that orients an initial angle (i.e. $\cot \phi = \cot \phi_0 + \gamma$; e.g., Platt, 1984). In the latter case, estimated simple shear strain varies dependent on an initial direction of the line (ϕ_0). We estimated the amount of simple shear strain for both cases in Fig. 10, where the initial angle of the material line was assumed to be $\phi_0 = 60^\circ$ after Fig. 8C as an example.

Fig. 10 shows the evolution of two parameters with respect to progressive simple shear strain. Fig. 10A shows that the intra-layer shear band cleavages have been progressively rotated from 10° to -20° as strain increased to $\gamma = 2$ (see also Fig. 8D). The direction of the shear band cleavages appears to become relatively stable at an angle oblique to the shear

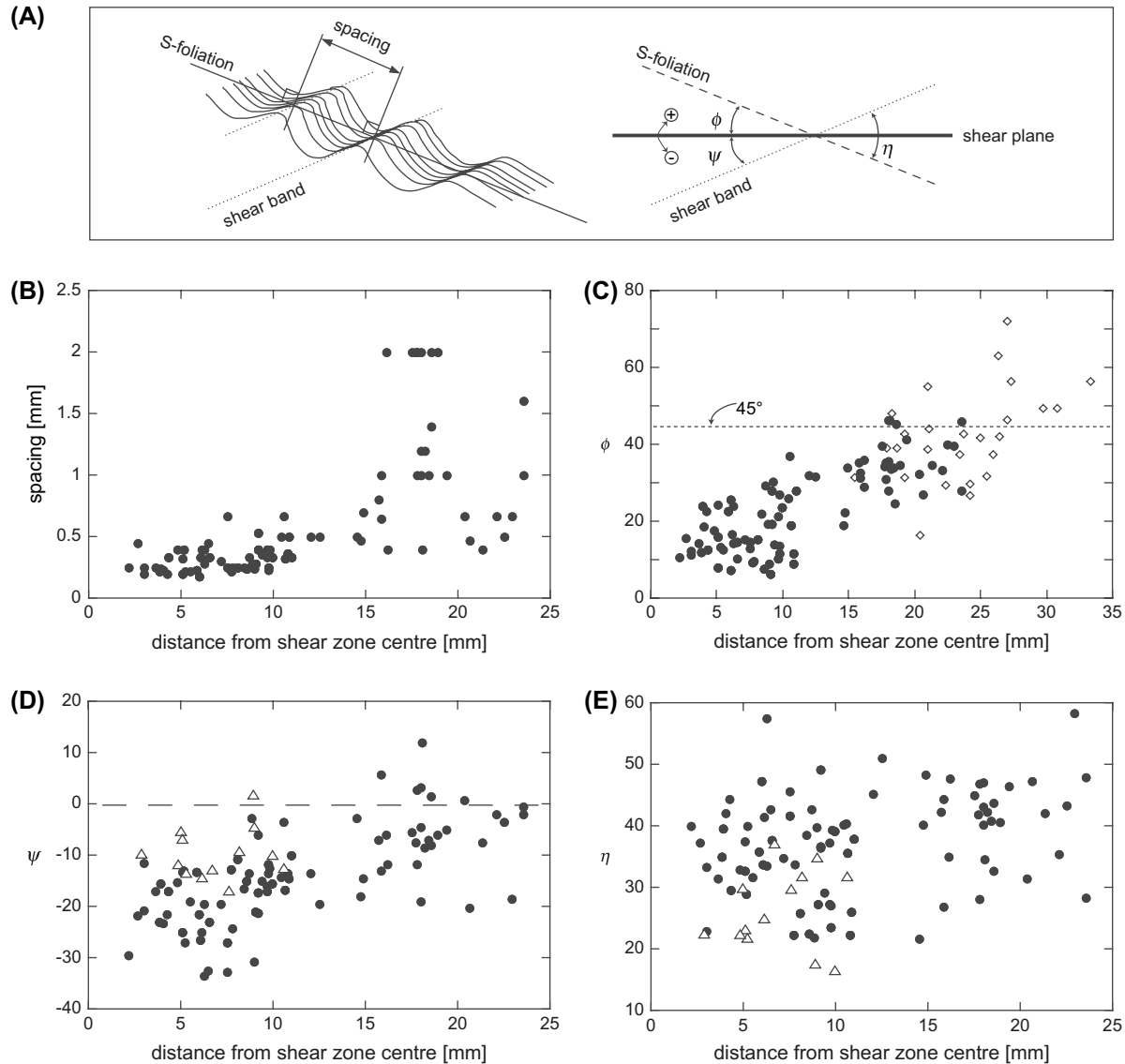


Fig. 8. (A) Measured parameters for geometric analysis: three angles and spacing with respect to the S-foliation, the intra-layer shear band cleavage (labelled as shear band) and the shear plane. (B) The spacing data with respect to the distance from the shear zone centre. (C) The angle between the S-foliation and the shear plane with respect to the distance from the shear zone centre. (D) The angle between the shear band cleavages and the shear plane. (E) The angle between the S-foliation and the shear band cleavages. Open diamonds indicate data from the biotite-feldspar domains that do not contain shear band cleavages. Solid circles indicate data from the biotite-feldspar domains that contain the intra-layer shear band cleavages. Open triangles show data from the biotite-feldspar domains that contain the inter-layer shear band cleavages.

plane regardless of simple shear strain (Fig. 10A). The angle between the S-foliation and the intra-layer shear band cleavage decreases gradually from 50° to 20° as strain reaches $\gamma = 9$ (Fig. 10B; cf. Fig. 8E).

Fig. 11 shows our interpretation of the development of the shear band cleavage based on the microstructural observations and the geometric analyses. An S-foliation developed first (Stage 0). As strain increased, the S-foliation was rotated and stretched, resulting in the formation of intra-layer shear band cleavage (Stage 1). In contrast to the S-foliation that occurred at high angle to the shear plane (i.e. ca. $\phi = 45^\circ$; Fig. 8C), the intra-layer shear band cleavage formed subparallel to the shear plane (i.e. ca. $\psi = 0$; Figs. 8D and 10A), where

the angle between the S-foliation and the intra-layer cleavage was as high as 50° (Figs. 8E and 10B). With increasing strain, the intra-layer shear band cleavages developed into discrete cleavages separated by microlithons (Stage 2a). As shown in Fig. 9, the angle η between the S-foliation and the shear band cleavage appears to be at around 40° at lower strain, whereas the S-foliation was rotated toward the shear plane. As strain increased further, the S-foliation rotated close to the shear plane, and the angle between the S-foliation and the shear band cleavage became smaller (Stage 2b; Figs. 8E and 10B). Finally, the inter-layer shear band cleavages cut across the intra-layer shear band cleavages that contain mainly Stage 2b microstructures (Stage 3).

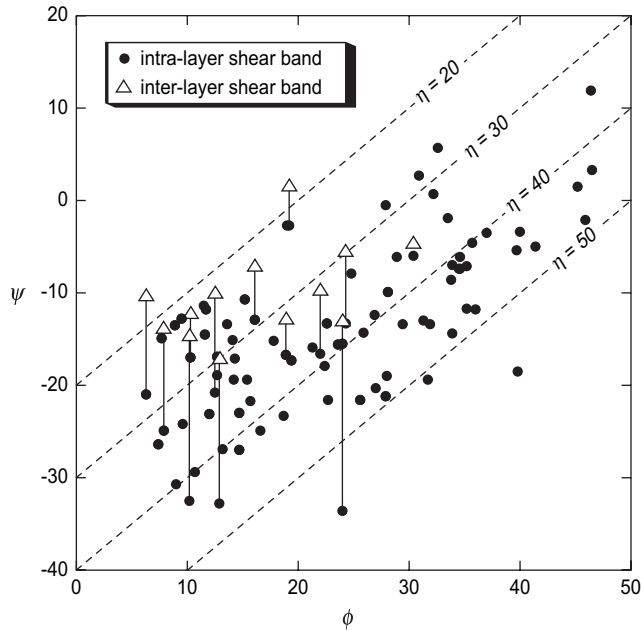


Fig. 9. A diagram showing the angular relationships among the S-foliation, the intra-layer and the inter-layer shear band cleavages with respect to the shear plane. Solid circles indicate the data for the intra-layer shear band cleavages, whereas open triangles indicate those for the inter-layer shear band cleavages. Each line between solid circle and open triangle shows a cross-cutting relationship between the intra-layer shear band cleavage and the inter-layer shear band cleavage. Broken lines indicate a constant angle (η) between the S-foliation and the shear band cleavages.

5.2. A finite strain ellipse model for the intra-layer shear band cleavages

Numerous models of the origin and evolution of planar fabrics in shear zones have been proposed (e.g., Ramsay, 1967, 1980; Berthé et al., 1979; Platt and Vissers, 1980; Platt, 1984; Lister and Snoke, 1984; Bobyarchick, 1986; Dennis and Secor, 1987, 1990; Passchier, 1991; Blenkinsop and Treloar, 1995; Pray et al., 1997). The different models predict different relationships between the bulk strain ellipsoid and the foliation (Blenkinsop and Treloar, 1995). For example, several studies describe the formation of S-fabrics parallel to the long axis of the finite strain ellipse in simple shear (e.g., Ramsay, 1967, 1980; Berthé et al., 1979; Lister and Snoke, 1984; Blenkinsop and Treloar, 1995). However, Platt (1984) suggested that slip could occur parallel to S-fabrics due to strain partitioning in overall simple shear (cf. Dennis and Secor, 1987, 1990).

With respect to shear band cleavages, Bobyarchick (1986) suggested that the inclined eigenvector may represent the orientation of shear bands in natural shear zones. Pray et al. (1997) showed that if the shear-surface was parallel to such an inclined eigenvector in a convergent shear zone, the S- and C-surfaces developed stable orientations and ceased to rotate. However, Simpson and De Paor (1993) argued that the eigenvector direction is an unstable direction, and once a plane is deflected slightly from this orientation, it will continue to rotate away from the eigenvector. Simpson and De

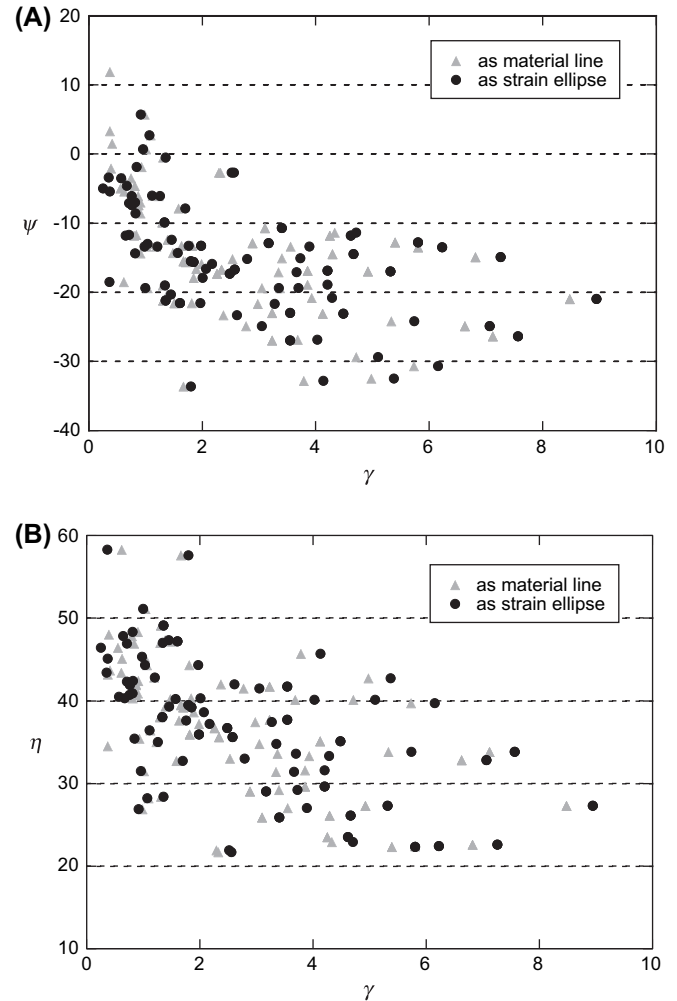


Fig. 10. (A) The angles (ψ) between the shear plane and the intra-layer shear band cleavages with respect to simple shear strain. (B) The angles (η) between the S-foliation and the intra-layer shear band cleavages with respect to simple shear strain. Shear strains were calculated from the angle (ϕ) between the S-foliation and the shear plane according to two assumptions: (i) ϕ being the material line of a simple shear strain ellipse and the initial angle of the material line: $\phi_0 = 60^\circ$ (gray triangles) and (ii) ϕ being the long axis of the simple shear strain ellipse (solid circles).

Paor (1993) favored a model in which shear bands propagate along surfaces close to the direction of maximum shear strain rate (see also Platt and Vissers, 1980; Ramsay and Lisle, 2000). In contrast, Blenkinsop and Treloar (1995) noted a geometrical similarity between shear surfaces in 'brittle shear zones' and S–C mylonites, and proposed that shear band cleavages form in the orientation of a Coulomb failure surface at an angle of less than 45° to the maximum principal stress.

Our data revealed that the intra-layer shear band cleavages could be progressively rotated with increasing strain (Fig. 10). Therefore, it appears that any fabric attractor models may not explain the rotation of the intra-layer shear bands, as the eigenvector direction parallel to the shear plane is thought to be the convergent direction for both positive and negative angles of foliation to the shear plane. On the contrary, a model with respect to the finite strain ellipse may be able to describe their rotational behavior, since it is well known that the

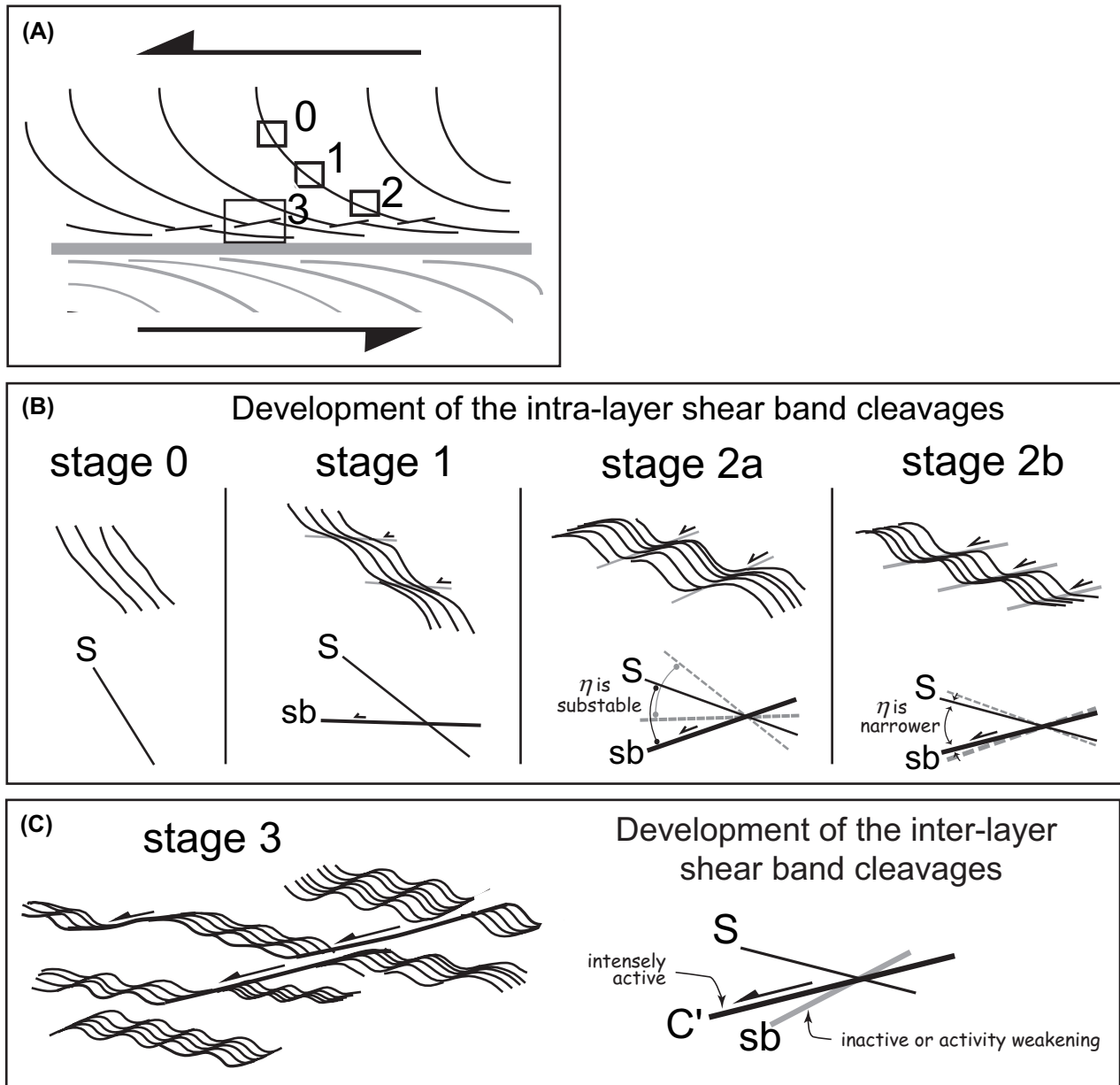


Fig. 11. Schematic diagram illustrating the development of intra-layer and inter-layer shear band cleavages. (A) Approximate location for each stage with respect to the shear zone. (B) Stage 0: initiation of S-foliation. Stage 1: the intra-layer shear band cleavages were progressively developed and rotated toward the shear plane, while the angle (η) between the S-foliation and the cleavage was substable. Stage 2a: the intra-layer shear band cleavages were intensely developed but were not much rotated toward the shear plane, while the angle (η) between the S-foliation and the cleavage decreased. Stage 2b: the intra-layer shear band cleavages were intensely developed but were not much rotated toward the shear plane, while the angle (η) between the S-foliation and the cleavage decreased. (C) Stage 3: the inter-layer shear band cleavages were developed, where the angles (ψ) between the shear plane and the intra-layer shear band cleavages tend to be larger (i.e. Fig. 9). Where the inter-layer shear band cleavages occur, the intra-layer shear band cleavages became largely or completely inactive.

rotational component of the finite strain ellipse exceeds the stretching component at lower strains, and subsequently its stretching component becomes dominant (e.g., Ramsay and Huber, 1983).

Another important feature of the data is that the intra-layer shear band cleavages became more discrete, where the spacing of the cleavage was nearly stable (Fig. 8B). This means that shearing along the cleavages became dominant with increasing strain. Ramsay and Lisle (2000) suggested that shear band cleavages develop as a result of shear instability early during deformation, but once formed, they guide successive shear

instabilities into the pre-existing shear band. However, although Ramsay and Lisle (2000) proposed that the shear bands will be oriented close, but not parallel to the position of maximum finite shear strain at any stage of deformation, our model shown below works in terms of passive rotation of previously formed material lines. Therefore, the orientations of the cleavages are not related to the position of maximum finite shear strain at any stage.

Ishii (1992) investigated theoretical deformation paths in layered rock masses and showed that layers with viscosity contrast deform by different amounts of non-coaxiality; layers

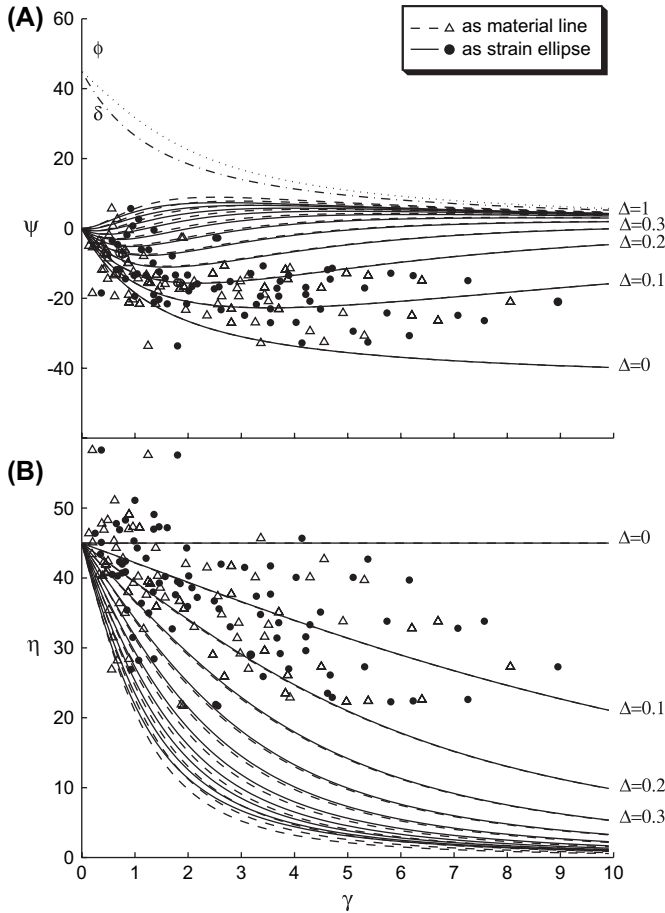


Fig. 12. Diagrams comparing the rotation of several material lines of strain ellipse in simple shear on a model presented in this paper and the data in Fig. 10. Shear strains were calculated from the angle (ϕ) between the S-foliation and the shear plane according to two assumptions: (i) ϕ being the material line of a simple shear strain ellipse and the initial angle of the material line: $\phi_0 = 60^\circ$ (broken lines for theoretical calculation and open triangles for the data) and (ii) ϕ being the long axis of the simple shear strain ellipse (solid lines for theoretical calculation and solid circles for the data). Δ represents the proportion of the bulk simple shear strain (γ). See text for discussion.

with low viscosity tend to deform by simple shear, and layers with high viscosity tend to deform coaxially (see also Jiang, 1994; Ishii, 1996). In our study, the quartz domains may be good candidates for layers with low viscosity, where simple shear deformation is dominant. In contrast, the biotite-feldspar domains have relatively high viscosity due to mantled K-feldspar (Fig. 6), and deformed coaxially. In this way, a model originally proposed by Platt (1984) may demonstrate the rotational behavior of the intra-layer shear band cleavages as follows.

We consider that a shear band cleavage rotates as a passive marker with respect to coaxial stretching (E^S), which is:

$$\tan \eta = \tan \eta_0 \left(\frac{1}{E^S} \right)^2, \quad (1)$$

where E^S is parallel to the S-foliation (Platt, 1984) and $\eta = \phi - \psi$ as defined in Fig. 8A. E^S can be defined as a function of the maximum strain (E_1). In simple shear,

$$\left(\frac{1}{E^S} \right)^2 = \left(\frac{1}{E_1} \right)^2 \cos^2 \beta + \left(\frac{1}{E_2} \right)^2 \sin^2 \beta, \quad (2)$$

$$(E_1)^2 = \frac{1}{2} \left[\gamma^2 + 2 + \gamma \sqrt{\gamma^2 + 4} \right], \quad (3)$$

where $E_2 = 1/E_1$ and $\beta = \delta - \phi$ (Ramsay, 1967; Platt, 1984). The parameter δ is the angle between E_1 and the shear plane, i.e.

$$\tan 2\delta = 2/\gamma. \quad (4)$$

With respect to the relationship between simple shear strain (γ) and the S-foliation (ϕ), there are two expressions depending on how we deal with the direction of the S-foliation. If we assume that the S-foliation rotates as a passive marker in simple shear, then

$$\cot \phi = \cot \phi_0 + \gamma. \quad (5)$$

Alternatively, if we assume that the S-foliation is parallel to the maximum stretching axis of a strain ellipsoid, then

$$\phi = \delta. \quad (6)$$

Here, we modified Eq. (3) further to:

$$(E_1)^2 = \frac{1}{2} \left[\Gamma^2 + 2 + \Gamma \sqrt{\Gamma^2 + 4} \right], \quad (7)$$

where

$$\Gamma = \Delta \gamma (0 \leq \Delta \leq 1). \quad (8)$$

Δ represents the proportion of the bulk simple shear strain (γ), which defines an effective simple shear strain (Γ) for coaxial stretching. In this model, the rotation rate of the strain ellipse is the same as that of the simple shear strain ellipse, while the stretching rate varies from the simple shear strain ellipse according to the value of Δ . For instance, if $\Delta = 1$, then $\Gamma = \gamma$, which follows the path of the simple shear strain ellipse. If $\Delta = 0$ and $\Gamma = 0$, such that the S-foliation accommodates no strain, then rotation of the shear band cleavages occurs at the same rate as that of the S-foliation.

Fig. 12A shows a series of rotation paths for ψ with respect to Δ and γ . When $\Delta = 1$, the stretching component is dominant and only minor rotation occurs at low strain. The parameter ψ is closer to 0 as strain increases (i.e. shear band cleavages become closer to the shear plane). In contrast, as Δ decreases, the rotation component is dominant over the stretching component, such that ψ decreases rapidly at lower strain and becomes stable. Fig. 12B shows evolution paths for η with respect to Δ and γ . In the case of simple shear ($\Delta = 1$), η decreases rapidly at low strains ($\gamma < 2$ in Fig. 12B) because of the effect of intense stretching. However, as Δ approaches 0, the rate of decrease in η is reduced.

Comparing the model results with our data, the paths that represent $0.1 \leq \Delta \leq 0.2$ appear to agree with the data. This suggests that internal strain within the biotite-feldspar domains may represent as little as 10–20% of the bulk simple

shear strain, suggesting that the kinematic development of intra-layer shear bands may be a response to very local kinematic conditions and not the bulk shear. Such local strains within the biotite-feldspar domains can be explained by their microstructural features; they are mantled by K-feldspar (Figs. 5 and 6). Thereby, the biotite-feldspar domains could not be intensely deformed during shearing, even though biotite grains occur in the domains. The majority of strain may be therefore accommodated with deformation in the quartz domains. It suggests that the development of the shear zone resulted in strain partitioning between the quartz and the biotite-feldspar domains. The shear zone occurs within the metasomatic biotite band in the granite. The development of the shear zone resulted in strain partitioning between the quartz and the biotite-feldspar domains due to compositional variations that occurred by hydrothermal alteration within the granite.

5.3. Development of the inter-layer shear band cleavages

Inter-layer shear band cleavages cut across both the S-foliation and the intra-layer shear band cleavages, and influenced plastic flow in the quartz domain (Fig. 5: curved quartz domains). This suggests that the inter-layer shear band cleavages occurred late during the development of the shear zone, and are, therefore, comparable with shear band cleavages reported by many researchers. Also, angles between the inter-layer shear band cleavages and the shear plane are relatively stable at -5° to -10° , suggesting that they underwent little rotation during bulk simple shearing. The orientation of shear band cleavages has previously been suggested as representing either the inclined eigenvector during sub-simple shear flow (e.g., Boryarchick, 1986; Pray et al., 1997), the direction of the maximum rate of shear strain (e.g., Platt and Vissers, 1980; Simpson and De Paor, 1993) or the orientation of a Coulomb failure surface at an angle of less than 45° to the maximum principal stress (Blenkinsop and Treloar, 1995). The first two models seem to require a stable homogeneous flow. Therefore, it is difficult to apply them for the inter-layer shear band cleavages in this study, as they appear to occur within the region of strain partitioning (see above). There is also no positive evidence to support the third model.

The inter-layer shear band cleavages occur where the orientation of intra-layer shear band cleavages became at a higher angle to the shear plane at higher strains (Fig. 9). This suggests that shearing along the intra-layer shear band cleavages may have ceased as their orientations became unsuitable to accumulate shear strain along them. Therefore, it is likely that the inter-layer shear band cleavages developed in those parts of the shear zone where increasing bulk shear strain prevented efficient strain partitioning between the quartz and the biotite-feldspar domains.

6. Conclusions

Microstructural analyses of shear band cleavages in a centimeter-scale shear zone within a metasomatic biotite band in the Teshima granite, Ryoke metamorphic belt, southwest Japan show that strain partitioning occurred between quartz and

biotite-feldspar domains within the shear zone. Pre-tectonic hydrothermal alteration within the granite caused biotite replacement of both plagioclase and K-feldspar, resulting in the development of biotite-feldspar domains where K-feldspar mantles dominantly biotite-plagioclase aggregate. Subsequently, the altered granite was plastically deformed in simple shear, so that intra-layer shear band cleavages were passively developed within the biotite-feldspar domains, whereas intense dynamic recrystallization occurred in the quartz domains. The rotation and orientation of the intra-layer shear band cleavages can be explained by a finite strain ellipse model. The model shows that strain in the biotite-feldspar domain requires only 10–20% of the bulk simple shear strain for the development of such cleavages, whereas most of strain could be accommodated by deformation in the quartz domains. Consequently, the model suggests that the development of the shear zone resulted in strain partitioning between the quartz and the biotite-feldspar domains due to compositional variations that occurred by hydrothermal alteration within the granite.

Acknowledgments

We acknowledge K. Ishii, D. T. Secor, E. Druguet, A. Lin, D. Gapais, and A. Stallard for their critical comments on an earlier version of this paper, and A. Stallard of University of Canterbury for improving the English in this paper. This paper was supported by the JSPS Postdoctoral fellowships for Research Abroad, and Research in Aids from the Japan Society of the Promotion of Science.

References

- Arita, M., 1988. Petrographical studies on granitic rocks in the Kojima Peninsula and Shiwaku islands, the central parts of Seto inland sea, southwest Japan: proterogenetic and magmatogenetic origin of granitic rocks. *Journal of the Geological Society of Japan* 94, 279–293.
- Berthé, D., Choukroune, P., Jegouzo, P., 1979. Orthogneiss, mylonite and non-coaxial deformation of granites: the example of the South Armorican shear zone. *Journal of Structural Geology* 1, 31–42.
- Blenkinsop, T.G., Treloar, P.J., 1995. Geometry, classification and kinematics of S–C fabrics. *Journal of Structural Geology* 17, 397–408.
- Boryarchick, A.R., 1986. The eigenvalue of steady flow in Mohr space. *Tectonophysics* 122, 35–51.
- Dennis, A.J., Secor, D.T., 1987. A model for the development of crenulations in shear zones with applications from the Southern Appalachian Piedmont. *Journal of Structural Geology* 9, 809–817.
- Dennis, A.J., Secor, D.T., 1990. On resolving shear direction in foliated rocks deformed by simple shear. *Bulletin of the Geological Society of America* 102, 1257–1267.
- Gapais, D., White, S.H., 1982. Ductile shear bands in a naturally deformed quartzite. *Textures and Microstructures* 5, 1–17.
- Hara, I., Takeda, K., Kimura, T., 1973. Preferred lattice orientation of quartz in shear deformation. *Journal of Science, Hiroshima University, Series C* 7, 1–10.
- Ishii, K., 1992. Partitioning of non-coaxiality in deforming layered rock masses. *Tectonophysics* 210, 33–43.
- Ishii, K., 1996. Partitioning of flow and progressive deformation of layered rock masses. *Tectonics and Metamorphism (The Hara Volume)*. SOUBUN Co., Ltd., Tokyo, pp. 296–303 (in Japanese with English abstract).
- Jiang, D., 1994. Flow variation in layered rocks subjected to bulk flow of various kinematic vorticities: theory and geological implications. *Journal of Structural Geology* 16, 1159–1172.

- Lister, G.S., Snoke, A.W., 1984. S–C mylonites. *Journal of Structural Geology* 6, 617–638.
- Michibayashi, K., Togami, S., Takano, M., Kumazawa, M., Kageyama, T., 1999. Application of scanning X-ray analytical microscope for the petrographic characterization in a shear zone: an alternative method to image microstructures. *Tectonophysics* 310, 55–67.
- Passchier, C.W., 1991. Geometric constraints on the development of shear bands in rocks. *Geologie en Mijnbouw* 70, 203–211.
- Passchier, C.W., Trouw, R.A., 2005. *Microtectonics*. Springer, p. 366.
- Platt, J.P., 1984. Secondary cleavages in ductile shear zones. *Journal of Structural Geology* 6, 439–442.
- Platt, J.P., Vissers, R.L.M., 1980. Extensional structures in anisotropic rocks. *Journal of Structural Geology* 2, 397–410.
- Pray, J.R., Secor Jr., D.T., Maher Jr., H.D., 1997. Rotation of fabric elements in convergent shear zones, with examples from the southern Appalachians. *Journal of Structural Geology* 19, 1023–1036.
- Ramsay, J.G., 1967. *Folding and Fracturing of Rocks*. MacGraw Hill, New York.
- Ramsay, J.G., 1980. Shear zone geometry: a review. *Journal of Structural Geology* 2, 83–99.
- Ramsay, J.G., Graham, R.H., 1970. Strain variation in shear belts. *Canadian Journal of Earth Sciences* 7, 786–813.
- Ramsay, J.G., Huber, M.I., 1983. Strain Analysis. In: *The Techniques of Modern Structural Geology*, vol. 2. Academic Press, London.
- Ramsay, J.G., Lisle, R.J., 2000. Applications of Continuum Mechanics in Structural Geology. In: *The Techniques of Modern Structural Geology*, vol. 3. Academic Press, London.
- Simpson, C., De Paor, D.G., 1993. Strain and kinematics analysis in general shear zones. *Journal of Structural Geology* 15, 1–20.
- Togami, S., Takano, M., Kumazawa, M., Michibayashi, K., 2000. An algorithm for the transformation of XRF images into mineral-distribution maps. *Canadian Mineralogist* 38, 1283–1294.
- White, S.H., Burrows, S.E., Carreras, J., Shaw, N.D., Humphreys, F.J., 1980. On mylonites in ductile shear zones. *Journal of Structural Geology* 2, 175–187.